Chapter 9
Modelling of a Hydrogen Saturated Layer Within the Micropolar Approach

Ksenia Frolova, Elena Vilchevskaya, Vladimir Polyanskiy & Ekaterina Alekseeva

Abstract This paper is concerned with modeling the strongly inhomogeneous hydrogen distribution over a sample by means of the micropolar continuum approach. The presence of micro-cracks covering the lateral surface of the sample is modeled by means of a distributed couple stress prescribed as a boundary condition. The applied couple stress produces a longitudinal displacement in return, which quickly fades away from the surface. The tensile displacement increases the intergranular space in the vicinity of the sample boundary and initiates hydrogen absorption from the environment. A comparison between widths of the surface layer that were experimentally determined and the ones that were analytically obtained allows estimating a value of one of the non-classical elastic parameters.

9.1 Introduction

Modern materials operate under extreme loads and in corrosive environments. The combined effect leads to stress corrosion cracking in metals (Jones, 2017), as well as to hydrogen-induced embrittlement (Koyama et al, 2012; Kyoung et al, 2009; Zhang et al, 2015). Experiments based on mass spectrometry and electron microscopy show that water vapor in the air is a source of hydrogen and that, in turn, the hydrogen leads to a decrease of strength, crack resistance and endurance lim-

Ksenia Frolova · Elena Vilchevskaya · Vladimir Polyanskiy
Institute for Problems in Mechanical Engineering RAS, Bolshoy pr., 61, V.O., St. Petersburg 199178 & Peter the Great St. Petersburg Polytechnic University, Polytechnicheskaya, 29, St. Petersburg 195294, Russia,
e-mail: kspfrolova@gmail.com, vilchevska@gmail.com, vapol@mail.ru

Ekaterina Alekseeva
Peter the Great St. Petersburg Polytechnic University, Polytechnicheskaya, 29, St. Petersburg 195294, Russia,
e-mail: alexeeva__ekaterina@mail.ru

B. E. Abali et al. (eds.), *New Achievements in Continuum Mechanics and Thermodynamics*, Advanced Structured Materials 108,
https://doi.org/10.1007/978-3-030-13307-8_9

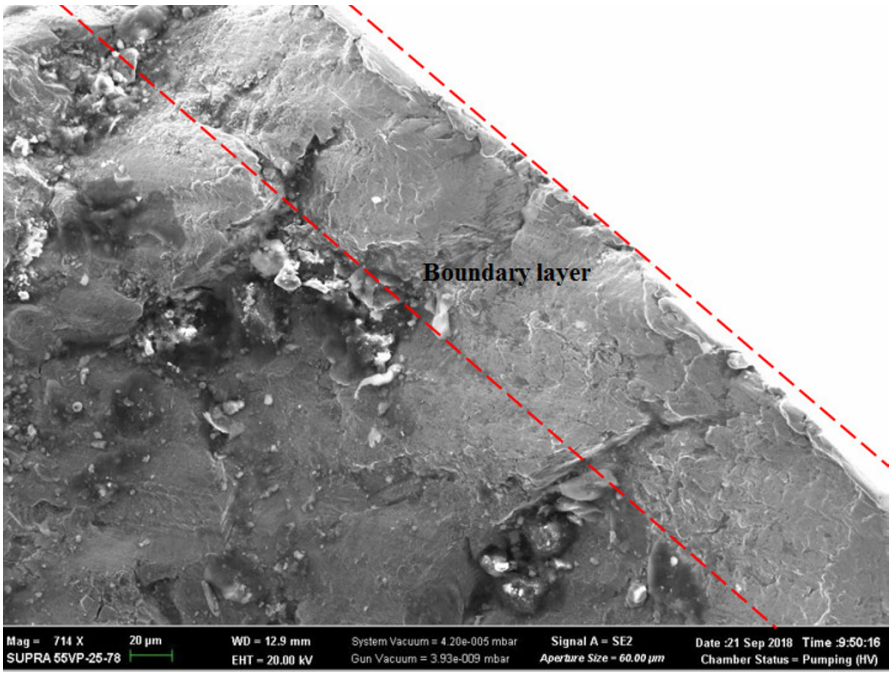

Fig. 9.1 Fractography of the sample after hydrogenation and fatigue test

its (Khrustalev et al, 1989). These effects are observed in samples saturated with hydrogen made from different types of materials, namely nickel, titanium, copper, aluminum alloys, and steel.

A number of articles were devoted to the investigation of hydrogen accumulation inside metals placed in an aggressive environment (Hadam and Zakroczymski, 2009; Martinsson and Sandström, 2012; Omura et al, 2016; Wu et al, 2015; Yagodzinskyy et al, 2011). Direct measurements of hydrogen concentrations, as well as mathematical modeling of hydrogen accumulation, show that the hydrogen is unevenly distributed and that there is a significant excess of its concentration within a thin boundary layer of the metal (Martinsson and Sandström, 2012; Wu et al, 2015). A highly heterogeneous distribution of hydrogen within the samples is also observed when fatigue test are performed with non-hydrogen-charged samples placed in air environment (Belyaev et al, 2017a,b). In Fig. 9.1 the fractography of a sample made of alloy 718 after hydrogen charging and fatigue test is shown. In this case, the hydrogen concentration in a thin boundary layer with an approximate thickness of about 100 µm exceeds 10–100 times the volumetric concentration.

It is known that the lateral surfaces of samples are covered with fractal oriented dislocations that, in turn, lead to micro-crack formation as in Betekhtin et al (2009); Kramer et al (2005); Steffens et al (1987). Detailed examinations of the surface layer in Steffens et al (1987) show that its grains or parts of a uniform mono-crystal rotate

and create empty spaces near the boundary. These additional empty spaces initiate the seepage of hydrogen from the external environment into the material. Thus, the non-homogeneous distribution of hydrogen over the sample can be explained by the existence of a lengthwise displacement appearing due to grain rotations in the vicinity of the lateral surface.

In other words, the theoretical interpretation of this phenomena should be connected with the material inner structure, in particular, with introduction of the intrinsic length scale parameter characterizing the width of the surface layer with a high hydrogen concentration. The dependence of mechanical response on the structure size could not be explained by the classical continuum mechanics since no length scale enters the constitutive equations. However, different generalized continuum theories have been successful in addressing a size effect problem. Examples for generalized continuum theories are the strain-gradient-theory as in Aifantis (1984); dell'Isola and Seppecher (1997); dell'Isola et al (2012), the micropolar theory as in Eringen and Kafadar (1976); Eremeyev et al (2012), and the surface-theory as in Altenbach et al (2010); Eremeyev and Pietraszkiewicz (2014), just to mention the most popular ones. A modern comparison of the different modelling options, which must be driven by phenomenology, can be found in dell'Isola et al (2017). In the present paper we are going to use a micropolar medium theory. As the first attempt to start the description and see how that approach works we will restrict ourself to isotropic linear continuum. A detailed discussion about other possible constitutive choices can be found in Eremeyev and Pietraszkiewicz (2016, 2012). Also it should be noted that although direct consideration of the cracking process is beyond the scope of the paper, the initial presence of the surface dislocations and microcracks is modeled by means of a distributed couple stress on the lateral surface of the sample. As a result, it will be shown that the prescription of couple stresses on the boundary leads to the appearance of additional tensile displacements increasing the intergranular space within the thin surface layer and therefore initiating the highly heterogeneous distribution of hydrogen.

Considering more complicated models usually involves introducing new parameters. There are four additional isotropic elastic constants in micropolar theory. Three of them provide a sensitivity to the rotation gradient and the remaining one quantifies the degree of coupling between macro and micro-rotation. Both theoretical and experimental investigations have been undertaken in order to determine these material coefficients (Adomeit, 1968; Askar, 1972; Askar and Cakmak, 1968; Ellis and Smith, 1967; Gauthier and Jahsman, 1975; Lake, 1983, 1995; Liebold and Müller, 2015, 2016; Perkins and Thompson, 1973; Schijve, 1966; Yang and Lakes, 1981). However, the accomplished work is still far from being complete and these coefficients are obtained only for a few different materials, namely, graphite, human bone, and foams. A comparison between the thickness of the high hydrogen concentration layer observed in experiments and the width of the layer with the analytically obtained tensile displacements allows for an estimate of the value of one of the non-classical elastic constants. This will be demonstrated in the last section for the aluminum alloy D16.

9.2 Basic Equations of Micropolar Media

Let us consider a geometrically linear micropolar continuum. Its deformations are described by the standard displacement field, $\boldsymbol{u}$, and an independent microrotation vector, $\boldsymbol{\theta}$. Then the stretch tensor $\boldsymbol{e}$ and wryness tensor $\boldsymbol{\kappa}$ can be introduced in the following way[1] (Eremeyev et al, 2012):

$$\boldsymbol{e} = \nabla \otimes \boldsymbol{u} + \boldsymbol{I} \times \boldsymbol{\theta}, \tag{9.1}$$

$$\boldsymbol{\kappa} = \nabla \otimes \boldsymbol{\theta}, \tag{9.2}$$

where ∇ is the gradient operator, and $\mathbf{I}$ is the unit tensor.

Note that the microrotation vector $\boldsymbol{\theta}$ is kinematically distinct from the "macrorotation," $\boldsymbol{w}$, determined by the antisymmetric part of the displacement gradient:

$$\boldsymbol{w} = \frac{1}{2} \nabla \times \boldsymbol{u}. \tag{9.3}$$

The vector $\boldsymbol{\theta}$ refers to the rotation of body particles, whereas $\boldsymbol{w}$ refers to the rotation associated with translational motion of nearby body particles. Thus, the decomposition of the stretch tensor into symmetric and antisymmetric parts yields

$$\boldsymbol{e} = \boldsymbol{\epsilon} + \boldsymbol{I} \times (\boldsymbol{\theta} - \boldsymbol{w}), \tag{9.4}$$

where $\boldsymbol{\epsilon} = 1/2(\nabla \otimes \boldsymbol{u} + \boldsymbol{u} \otimes \nabla)$ is the strain tensor of classical linear elasticity.

The constitutive equations for the stress tensor $\boldsymbol{T}$ and the couple stress tensor $\boldsymbol{M}$ for linear isotropic Cosserat elasticity are as follows (Eringen and Kafadar, 1976):

$$\boldsymbol{T} = \lambda \left(\nabla \cdot \boldsymbol{u}\right) \boldsymbol{I} + 2\mu\boldsymbol{\epsilon} + \gamma \boldsymbol{I} \times (\boldsymbol{\theta} - \boldsymbol{w}), \tag{9.5}$$

$$\boldsymbol{M} = \beta_1 \left(\nabla \cdot \boldsymbol{\theta}\right) \boldsymbol{I} + \beta_2 \boldsymbol{\kappa}^\top + \beta_3 \boldsymbol{\kappa}, \tag{9.6}$$

where λ, μ, γ and β_i $(i = 1, 2, 3)$ are independent elastic moduli. λ and μ are the classical elastic moduli, and γ is a modulus quantifying the degree of coupling between macro and micro rotation fields. The elastic moduli β_2 and β_3 allow to introduce material lengths reflecting effects of the couple stress, for example, $l_t = \sqrt{(\beta_2 + \beta_3)/2\mu}$ for torsion, or $l_b = \sqrt{\beta_3/4\mu}$ for bending (see, for example, Gauthier and Jahsman (1975)). When these length parameters vanish, the solutions obtained from couple stress theory reduce to those of classical elasticity theory. In perfect crystals and amorphous materials l_b and l_t are probably submicroscopic; but might be of the order of the averaged radius of roots of surface cracks (Mindlin, 1964).

The displacement and microrotation vectors can be found from the equilibrium equations, that in case of absence of body forces and body couples are

[1] A cross product between a second-rank tensor $\boldsymbol{A} = \boldsymbol{a}_k \boldsymbol{b}_k$ and vector $\boldsymbol{c}$ is realized in the following way: $\boldsymbol{A} \times \boldsymbol{c} = \boldsymbol{ab} \times \boldsymbol{c} = \boldsymbol{a}\,(\boldsymbol{b} \times \boldsymbol{c})$, i.e. the second vector in the tensor dyad is attached with the vector $\boldsymbol{c}$.

$$\nabla \cdot \boldsymbol{T} = 0. \tag{9.7}$$

$$\nabla \cdot \boldsymbol{M} + \boldsymbol{T}_{\times} = 0, \tag{9.8}$$

where $(\boldsymbol{a} \otimes \boldsymbol{b})_{\times} = \boldsymbol{a} \times \boldsymbol{b}$.

Within the framework of this paper we shall consider a case in which $\gamma \to \infty$. This corresponds to a case in which the antisymmetric part of the stretch tensor goes to zero or, in other words, to an assumption that the macrorotation and microrotation vectors are equal. It follows that it is the medium with constrained rotation, and the microrotation is determined by the displacement:

$$\boldsymbol{\theta} = \frac{1}{2} \nabla \times \boldsymbol{u}. \tag{9.9}$$

This means that $\nabla \cdot \boldsymbol{\theta} = 0$ and therefore parameter β_1 does not play any role in this model. Then Eqn.(9.6) simplifies to

$$\boldsymbol{M} = \frac{1}{2} \left(\beta_3 \nabla \otimes (\nabla \times \boldsymbol{u}) + \beta_2 (\nabla \times \boldsymbol{u}) \otimes \nabla \right). \tag{9.10}$$

According to Eqn. (9.8) together with Eqns. (9.5), (9.10), (9.4), and (9.3) we can obtain the following equality:

$$\boldsymbol{T}_{\times} = -2\gamma(\boldsymbol{\theta} - \boldsymbol{w}) = -\beta_3 \triangle \boldsymbol{w}, \tag{9.11}$$

where $\triangle = \nabla \cdot \nabla$ is the Laplace operator.

Consequently, the antisymmetric part of the stress tensor can be rewritten as follows:

$$\boldsymbol{T}^A = \frac{\beta_3}{4} \triangle \left(\boldsymbol{u} \otimes \nabla - \nabla \otimes \boldsymbol{u} \right). \tag{9.12}$$

As a result we obtain the following equation for the displacement field:

$$(\lambda + \mu) \nabla (\nabla \cdot \boldsymbol{u}) + \mu \triangle \boldsymbol{u} + \frac{\beta_3}{4} \nabla \cdot \triangle \left(\boldsymbol{u} \otimes \nabla - \nabla \otimes \boldsymbol{u} \right) = 0. \tag{9.13}$$

9.3 Axially-symmetrical Problem

In this paper we model the behavior of a cylindrical sample made of metal in an aggressive environment. In this context let us consider a boundary-value problem in cylindrical coordinates (r, φ, z) dealing with a solid cylinder of radius r_0 and length L subjected to a distributed couple stress, $-M_0 \boldsymbol{e}_{\varphi}$, on its lateral surface. Whereas a zero displacement field satisfies the equilibrium conditions and guarantees a traction-free lateral surface, the applied couple stress on the lateral surface produces an additional displacement which is fading away quickly from the surface.

We assume that the problem is axially symmetric and look for a solution with the following ansatz:

$$\boldsymbol{u} = \boldsymbol{u}\,(r,z) = u_r\,(r,z)\,\boldsymbol{e}_r + u_z\,(r,z)\,\boldsymbol{e}_z, \tag{9.14}$$

where $\boldsymbol{e}_r$ is the radial unit vector, and $\boldsymbol{e}_z$ is the unit vector along the cylinder axis.

From Eqns. (9.9) and (9.14) it follows that the microrotation vector has only one component, namely

$$\boldsymbol{\theta} = \theta_\varphi \boldsymbol{e}_\varphi = \frac{1}{2}\left(\frac{\partial u_r}{\partial z} - \frac{\partial u_z}{\partial r}\right)\boldsymbol{e}_\varphi. \tag{9.15}$$

In order to obtain the solution for the boundary layer in closed form, we have to take the following inequalities into account:

$$\begin{aligned} \frac{\partial^2 u_r}{\partial z^2} &\ll \frac{\partial^2 u_r}{\partial r^2}, \\ \frac{\partial^2 u_z}{\partial z^2} &\ll \frac{\partial^2 u_z}{\partial r^2}, \\ \frac{\partial u_z}{\partial z} &\ll \frac{\partial^2 u_z}{\partial r^2}. \end{aligned} \tag{9.16}$$

Consequently, Eqn. (9.13) reduces to

$$\begin{aligned} \left[\lambda\left(\frac{\partial^2 u_r}{\partial r^2} + \frac{\partial^2 u_z}{\partial r \partial z}\right) + 2\mu\left(\frac{\partial^2 u_r}{\partial r^2} + \frac{1}{2}\frac{\partial^2 u_z}{\partial z \partial r}\right) - \frac{\beta_3}{2}\frac{\partial^3 \theta_\varphi}{\partial z \partial r^2}\right]\boldsymbol{e}_r + \\ \left[\lambda\frac{\partial^2 u_r}{\partial z \partial r} + \mu\left(\frac{\partial^2 u_z}{\partial r^2} + \frac{\partial^2 u_r}{\partial r \partial z}\right) + \frac{\beta_3}{2}\frac{\partial^3 \theta_\varphi}{\partial r^3}\right]\boldsymbol{e}_z = 0. \end{aligned} \tag{9.17}$$

Here the terms of higher order of smallness are discarded.

By introducing non-dimensional parameters

$$\begin{gathered} x = 1 - \frac{r}{r_0}, \quad \widetilde{z} = \frac{z}{L}, \quad \xi = \frac{r_0}{L}, \quad u_x = \frac{u_r}{r_0}, \quad u_{\widetilde{z}} = \frac{u_z}{L}, \\ \widetilde{\lambda} = \frac{\lambda}{\mu}, \qquad \delta = \sqrt{\frac{\beta_3}{4\mu r_0^2}} = \frac{l_b}{r_0}. \end{gathered} \tag{9.18}$$

we can rewrite Eqn. (9.17) by the following system of equations:

$$\begin{aligned} \left(\widetilde{\lambda}+2\right)\frac{\partial^2 u_x}{\partial x^2} - \left(\widetilde{\lambda}+1\right)\frac{\partial^2 u_{\widetilde{z}}}{\partial x \partial \widetilde{z}} - \delta^2 \frac{\partial^4 u_{\widetilde{z}}}{\partial x^3 \partial \widetilde{z}} = 0, \\ -\left(\widetilde{\lambda}+1\right)\frac{\partial^2 u_x}{\partial x \partial \widetilde{z}} + \frac{1}{\xi^2}\frac{\partial^2 u_{\widetilde{z}}}{\partial x^2} - \delta^2\left(\frac{1}{\xi^2}\frac{\partial^4 u_{\widetilde{z}}}{\partial x^4} + \frac{\partial^4 u_x}{\partial x^3 \partial \widetilde{z}}\right) = 0. \end{aligned} \tag{9.19}$$

By integrating the first equation, we obtain

$$\frac{\partial u_x}{\partial x} = \frac{\widetilde{\lambda}+1}{\widetilde{\lambda}+2}\frac{\partial u_{\widetilde{z}}}{\partial \widetilde{z}} + \frac{\delta^2}{\widetilde{\lambda}+2}\frac{\partial^3 u_{\widetilde{z}}}{\partial x^2 \partial \widetilde{z}}. \tag{9.20}$$

Then the second equation in (9.19) yields

$$u_{\widetilde{z}} - \delta^2 \frac{\partial^2 u_{\widetilde{z}}}{\partial x^2} = 0. \tag{9.21}$$

Since δ is of small value and the displacement has a finite value, we arrive at the following solution for $u_{\widetilde{z}}$:

$$u_{\widetilde{z}} = A\left(\widetilde{z}\right) \exp\Big(- \frac{x}{\delta}\Big). \tag{9.22}$$

The solution for the dimensionless radial displacement reads

$$u_x = -A'\left(\widetilde{z}\right) \delta \exp\Big(- \frac{x}{\delta}\Big). \tag{9.23}$$

By applying non-dimensional parameters, Eqn. (9.15) for the microrotations can be finally rewritten in the following way:

$$\theta_\varphi = \frac{1}{2\xi\delta} A(\widetilde{z}) \exp\Big(- \frac{x}{\delta}\Big). \tag{9.24}$$

As a result the stress tensor has the form

$$\widetilde{\boldsymbol{T}} = \frac{1}{\mu}\boldsymbol{T} = 2\exp\Big(- \frac{x}{\delta}\Big) \left(A'\left(\widetilde{z}\right) \left(\boldsymbol{e}_z \otimes \boldsymbol{e}_z - \boldsymbol{e}_r \otimes \boldsymbol{e}_r\right) + \frac{1}{\xi\delta} A\left(\widetilde{z}\right) \boldsymbol{e}_z \otimes \boldsymbol{e}_r \right). \tag{9.25}$$

Obviously, the smallness of the first two terms is of higher order than the last one and formally they can be disregarded. However, in order to be sure that the lateral surface is traction free we will treat $A(z)$ as a constant. Thus the couple stress is given by

$$\widetilde{\boldsymbol{M}} = \frac{1}{\mu L}\boldsymbol{M} = 2A \exp\Big(- \frac{x}{\delta}\Big) \left(\frac{\beta_2}{\beta_3} \boldsymbol{e}_\varphi \otimes \boldsymbol{e}_r - \boldsymbol{e}_r \otimes \boldsymbol{e}_\varphi \right). \tag{9.26}$$

From (9.26) we obtain the equation for the unknown constant:

$$\boldsymbol{e}_r \cdot \boldsymbol{M} \,|_{x=0} = -M_0 \boldsymbol{e}_\varphi, \qquad \rightarrow \qquad A = \frac{M_0}{2\mu L}. \tag{9.27}$$

So far we have considered a problem without external loads on the faces at the end. However, either axial tension

$$\boldsymbol{F} = F\boldsymbol{e}_z = \int_S T_{zz} \boldsymbol{e}_z \, \mathrm{d}S$$

or torsion

$$\boldsymbol{M}_t = M_t \boldsymbol{e}_z = \int_S (\boldsymbol{r} \times (\boldsymbol{e}_z \cdot \boldsymbol{T}) + M_{zz} \boldsymbol{e}_z) \, \mathrm{d}S$$

can be added. Here S is the cross-sectional area of the cylinder. The particular solutions of these Saint-Venant's problems are given by Gauthier and Jahsman (1975) and the total solutions for the medium with constrained rotation are

$$\begin{aligned} \boldsymbol{u} &= -\frac{\nu F r}{ES}\boldsymbol{e}_r + \left(\frac{Fz}{ES} + \frac{M_0}{2\mu}\exp\Big(-\frac{r_0 - r}{l_b}\Big)\right)\boldsymbol{e}_z, \\ \boldsymbol{T} &= \frac{F}{S}\boldsymbol{e}_z\boldsymbol{e}_z + \frac{M_0}{l_b}\exp\Big(-\frac{r_0 - r}{l_b}\Big)\boldsymbol{e}_z\boldsymbol{e}_r \end{aligned} \tag{9.28}$$

for tension and

$$\begin{aligned} \boldsymbol{u} &= C_1 r z \boldsymbol{e}_\varphi + \frac{M_0}{2\mu}\exp\Big(-\frac{r_0 - r}{l_b}\Big)\boldsymbol{e}_z, \\ \boldsymbol{T} &= C_1\mu r\left(\boldsymbol{e}_z\otimes\boldsymbol{e}_\varphi + \boldsymbol{e}_\varphi\otimes\boldsymbol{e}_z\right) + \frac{M_0}{l_b}\exp\Big(-\frac{r_0 - r}{l_b}\Big)\boldsymbol{e}_z\otimes\boldsymbol{e}_r, \\ \boldsymbol{M} &= C_1(\beta_2+\beta_3)\left(\boldsymbol{e}_z\otimes\boldsymbol{e}_z - \frac{1}{2}\left(\boldsymbol{e}_r\otimes\boldsymbol{e}_r + \boldsymbol{e}_\varphi\otimes\boldsymbol{e}_\varphi\right)\right) + \\ &+ M_0\exp\Big(-\frac{r_0 - r}{l_b}\Big)\left(\frac{\beta_2}{\beta_3}\boldsymbol{e}_\varphi\otimes\boldsymbol{e}_r - \boldsymbol{e}_r\otimes\boldsymbol{e}_\varphi\right), \\ C_1 &= \frac{M_t}{S}\left(\beta_2+\beta_3+\mu\frac{r_0^2}{2}\right)^{-1} \end{aligned} \tag{9.29}$$

for torsion. Here $\nu = \lambda/(2(\lambda+\mu))$ and $E = \mu(3\lambda+2\mu)/(\lambda+\mu)$ are Poisson's ratio and Young's modulus, respectively.

In both cases, the additional exponential terms play a role only within a thin surface layer and serves as a correction terms in order to satisfy the boundary condition on the lateral surface. Note that the torsion solution provided in Gauthier and Jahsman (1975) is traction-free on the lateral surface. However, in the case of the medium with constrained rotation it has a couple stress on the boundary:

$$M_{rr} = -\frac{C_1}{2}\left(\beta_2+\beta_3\right). \tag{9.30}$$

9.4 Results

As one can see from the previous section, considering a micropolar media allows us to obtain an additional displacement along the cylinder axis in the vicinity of the lateral surface. This tensile displacement increases the intergranular space and can initiate hydrogen absorption from the environment. In order to estimate the parameters of the model let us consider a cylindrical sample made of the aluminum alloy D16, because this material is frequently used in experiments in Andronov et al (2017). The following values will be used: $r_0 = 0.0045$ m, $L = 0.035$ m, $\mu = 27000$ MPa.

In order to estimate the small parameter δ we correlate the width of the layer with the additional displacements within the thickness of the boundary layer containing a higher concentration of hydrogen, x_*. Since u_z is exponentially decreasing from of the surface we define its limit value by $\chi u_{\tilde{z}}\,|_{x=0}$, where χ is a small parameter. Thus, the equation for δ can be written in the following way:

$$\delta = -\frac{x_*}{Ln(\chi)}. \tag{9.31}$$

When taking $x_* = 100\ \mu\text{m}/r_0 \approx 0.02$ and $\chi = 0.01$ we obtain $\delta \approx 0.005$. Recall that δ is related to the non-classic elastic modulus β_3 through Eqn. (9.18) as follows:

$$\beta_3 = 4\mu r_0^2 \delta^2. \tag{9.32}$$

Therefore, the elastic modulus can be estimated as: $\beta_3 \approx 5 \cdot 10^{-5}\,\text{MPa}\,\text{m}^2$.

The dependence of the displacement along the cylinder axis for this value of β_3 is shown in Fig. 9.2. The curve is plotted for $M_0 = -189$ kPa corresponding to $A = 0.0001$.

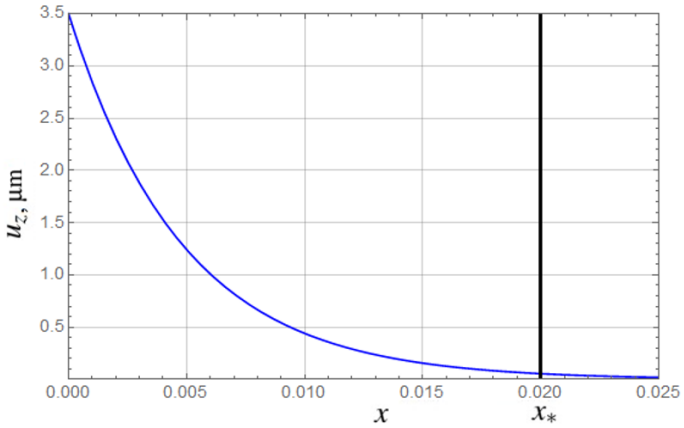

Fig. 9.2 Dependence of the tensile displacement on the relative distance from the lateral surface

9.5 Conclusions and Outlook

In this paper two main tasks were accomplished:

- First, an attempt was made to model the strongly inhomogeneous distribution of hydrogen observed in experiments within a micropolar continuum approach. The stress-strain state in the sample can be obtained within the theory of classical elasticity while the situation near the body surface could be depicted more

accurately by a solution, which is quickly fading away from the border. This solution gives additional tensile displacements in the vicinity of the lateral surface by means of which the absorption of hydrogen from the environment can be initiated. Note that we did not consider the hydrogen diffusion but concentrated on possible reasons of the hydrogen seepage.

- Second, a new method for estimating the additional elastic constants of a Cosserat medium was proposed. It is based on the comparison between the experimentally measured width of the surface layer containing the high hydrogen concentration and the analytically obtained characteristic length from the fading solution.

More research in this field is planned for the future in order to study the boundary layer emergence within Cosserat elasticity without restriction. At this stage a medium with constrained rotation was considered. The adopted simplification allowed us to obtain the analytical solution and to demonstrate feasibility of the suggested approach. However, the strong coupling between the macro and micro-rotations does not describe the rotation of grains in a proper manner and should be softened.

Moreover, it the displacement was supposed to be axially symmetric. This is a "classical" assumption for a cylindrical sample, but it limits the types of boundary condition to be prescribed at the lateral surface, namely, the distributed couple stress caused by microcracks. The microcracks distribution might be non-homogeneously over the sample surface and therefore leads to a dependence of the couple stress on the azimuth angle φ. Evidently a numerical approach will be required in that case.

In order to estimate the value of the non-classical elastic parameters, further efforts should be devoted to providing experiments with different materials and specimens sizes.

Acknowledgements Support of this work by a grant from Russian Science Foundation by RSF grant no. 18-19-00160 is gratefully acknowledged.

References

Adomeit G (1968) Mechanics of Generalized Continua (Edited by E. Kroner), chapter Determination of elastic constants of a structured material. lUTAM Symposia, Springer-Verlag Berlin Heidelberg

Aifantis EC (1984) On the microstructural origin of certain inelastic models. Journal of Engineering Materials and technology 106(4):326–330

Altenbach J, Altenbach H, Eremeyev VA (2010) On generalized Cosserat-type theories of plates and shells: a short review and bibliography. Archive of Applied Mechanics 80(1):73–92

Andronov DY, Arseniev DG, Polyanskiy AM, Polyanskiy VA, Yakovlev YA (2017) Application of multichannel diffusion model to analysis of hydrogen measurements in solid. International Journal of Hydrogen Energy 42(1):699–710

Askar A (1972) Molecular crystals and the polar theories of the continua experimental values of material coefficients for kno3. International Journal of Engineering Science 10(3):293–300

Askar A, Cakmak AS (1968) A structural model of a micropolar continuum. International Journal of Engineering Science 6(10):583–589

Belyaev AK, Grishchenko AI, Polyanskiy VA, Semenov AS, Tretyakov DA, Shtukin LV, Arseniev DG, A YY (2017a) Acoustic anisotropy and dissolved hydrogen as an indicator of waves of plastic deformation. In: Days on Diffraction, 2017, pp 39–44

Belyaev AK, Polyanskiy VA, Yakovlev YA, Mansyrev DE, Polyanskiy AM (2017b) Surface effect of the waves of plastic deformation and hydrogen distribution in metals. In: Days on Diffraction, 2017, pp 45–50

Betekhtin VI, Gilyarov VL, Kadomtsev AG, Korsukov VE, Korsukova MM, Obidov BA (2009) Fractalization of the surface relief of an amorphous alloy as an indication of rupture. Bulletin of the Russian Academy of Sciences: Physics 73(10):1419

dell'Isola F, Seppecher P (1997) Edge contact forces and quasi-balanced power. Meccanica 32(1):33–52

dell'Isola F, Seppecher P, Madeo A (2012) How contact interactions may depend on the shape of Cauchy cuts in Nth gradient continua: approach "à la D'Alembert". Zeitschrift für angewandte Mathematik und Physik 63(6):1119–1141

dell'Isola F, Corte AD, Giorgio I (2017) Higher-gradient continua: The legacy of Piola, Mindlin, Sedov and Toupin and some future research perspectives. Mathematics and Mechanics of Solids 22(4):852–872

Ellis RW, Smith CW (1967) A thin-plate analysis and experimental evaluation of couple-stress effects. Experimental Mechanics 7(9):372–380

Eremeyev VA, Pietraszkiewicz W (2012) Material symmetry group of the non-linear polar-elastic continuum. International Journal of Solids and Structures 49(14):1993–2005

Eremeyev VA, Pietraszkiewicz W (2014) Refined theories of plates and shells. ZAMM-Journal of Applied Mathematics and Mechanics/Zeitschrift für Angewandte Mathematik und Mechanik 94(1-2):5–6

Eremeyev VA, Pietraszkiewicz W (2016) Material symmetry group and constitutive equations of micropolar anisotropic elastic solids. Mathematics and Mechanics of Solids 21(2):210–221

Eremeyev VA, Lebedev LP, Altenbach H (2012) Foundations of micropolar mechanics. Springer Science & Business Media

Eringen AC, Kafadar CB (1976) Polar field theories. In: Continuum Physics, Volume 4, Elsevier, pp 1–73

Gauthier RD, Jahsman WE (1975) A quest for micropolar elastic constants. Journal of Applied Mechanics 42:369–374

Hadam U, Zakroczymski T (2009) Absorption of hydrogen in tensile strained iron and high-carbon steel studied by electrochemical permeation and desorption techniques. International Journal of Hydrogen Energy 34(5):2449–2459

Jones RH (2017) Stress-Corrosion Cracking, Materials performance and evaluation. ASM international

Khrustalev YA, Simakov YS, Glazunov MP, Gubin VV (1989) Formation of hydrogen under the metal friction (in russian). Russian Journal of Physical Chemistry A 63(5):1355–1357

Koyama M, Akiyama E, Tsuzaki K (2012) Hydrogen-induced delayed fracture of a fe–22mn–0.6 c steel pre-strained at different strain rates. Scripta Materialia 66(11):947–950

Kramer DE, Savage MF, Levine LE (2005) Afm observations of slip band development in al single crystals. Acta Materialia 53(17):4655–4664

Kyoung HS, Ji SK, Young SC, Kyung-Tae P, Young-Kook L, Chong SL (2009) Hydrogen delayed fracture properties and internal hydrogen behavior of a fe–18mn–1.5 al–0.6 c twip steel. ISIJ International 49(12):1952–1959

Lake R (1995) Experimental methods for study of Cosserat elastic solids and other generalized elastic continua. Continuum models for materials with microstructure pp 1–25

Lake RS (1983) Size effects and micromechanics of a porous solid. Journal of Materials Science 18(9):2572–2580

Liebold C, Müller WH (2015) Are microcontinuum field theories of elasticity amenable to experiments? a review of some recent results. In: Differential Geometry and Continuum Mechanics, Springer, pp 255–278

Liebold C, Müller WH (2016) Applications of higher-order continua to size effects in bending: Theory and recent experimental results. In: Generalized Continua as Models for Classical and Advanced Materials, Springer, pp 237–260

Martinsson A, Sandström R (2012) Hydrogen depth profile in phosphorus-doped, oxygen-free copper after cathodic charging. Journal of Materials Science 47(19):6768–6776

Mindlin RD (1964) Micro-structure in linear elasticity. Archive for Rational Mechanics and Analysis 16(1):51–78

Omura T, Nakamur J, Hirata H, Jotoku K, Ueyama M, Osuki T, Terunuma M (2016) Effect of surface hydrogen concentration on hydrogen embrittlement properties of stainless steels and ni based alloys. ISIJ International 56(3):405–412

Perkins RW, Thompson D (1973) Experimental evidence of a couple-stress effect. AIAA Journal 11(7):1053–1055

Schijve J (1966) Note on couple stresses. Journal of the Mechanics and Physics of Solids 14(2):113–120

Steffens T, Schwink C, Korner A, Karnthaler HP (1987) Transmission electron microscopy study of the stacking-fault energy and dislocation structure in cumn alloys. Philosophical Magazine A 56(2):161–173

Wu R, Ahlström J, Magnusson H, Frisk K, Martinsson A (2015) Charging, degassing and distribution of hydrogen in cast iron. Swerea KIMAB pp 1–41

Yagodzinskyy Y, Todoshchenko O, Papula S, Hänninen H (2011) Hydrogen solubility and diffusion in austenitic stainless steels studied with thermal desorption spectroscopy. steel research international 82(1):20–25

Yang JFC, Lakes RS (1981) Transient study of couple stress effects in compact bone: torsion. Journal of Biomechanical Engineering 103(4):275–279

Zhang S, Huang Y, Sun B, Liao Q, Lu H, Jian B, Mohrbacher H, Zhang W, Guo A, Zhang Y (2015) Effect of nb on hydrogen-induced delayed fracture in high strength hot stamping steels. Materials Science and Engineering: A 626:136–143